Table of Contents

1 Summary of Personnel and Work Efforts

The investigation and budget proposed here assumes the following commitments from the Principal Investigator and Co-Investigators. The efforts of GSFC Civil Servants and scientists resident at GSFC are expressed as full time equivalent fractions.

Investigator	**Affiliation**	**Budgeted FTEs**	
		FY2007	*FY2008*
Brian Dennis	GSFC	0.08	0.08
Philip Deines-Jones	GSFC	0.17	0.17
Kevin Black	Forbin Scientific	0.42	0.42

2 Scientific/Technical/Management

2.1 Objectives and Significance

The objective of this effort is to demonstrate the feasibility of a new photoelectric polarimetry technique that could serve as the basis of an instrument with sufficient polarization sensitivity and angular resolution in the 20-50 keV band to definitively test models of electron acceleration in solar flares. We anticipate that we would then leverage this effort to propose a balloon-borne mission for the next solar maximum to measure polarization in M- and X-class flares to accuracies of one per cent with 10 arc second imaging. This instrument would simultaneously provide imaging polarimetry, timing, and keV spectroscopy.

Our understanding of electron acceleration in solar flares remains fundamentally incomplete despite detailed spectral and temporal imaging of the resulting hard X-ray bremsstrahlung. Polarization measurements provide direct information on the degree of beaming of the accelerated electrons, an important aspect of particle acceleration models. Available measurements are tantalizing, but insufficient to distinguish between competing models.

A new technique for X-ray polarimetry, based on the photoelectric effect, has emerged in the last few years that could provide important new capabilities in the 20-50 keV band. This could serve as an important complement to Compton polarimeters, which remain more sensitive at energies above 50 keV. Recently, we demonstrated a new variant of this photoelectric technique that readily scales to the large effective areas required for hard X-ray imaging polarimetry with a rotating modulation collimator. We propose in this effort to demonstrate this large-area hard X-ray photoelectric polarimeter.

2.1.1 Scientific Motivation

Our knowledge of the hard X-ray bremsstrahlung produced in solar flares, a key diagnostic of electron acceleration, remains fundamentally incomplete. The temporal signature and spectrum have been studied for almost half a century, culminating in the unprecedented observations from the Reuven Ramaty High Energy Solar Spectroscopic Imager (RHESSI) [Lin 02]. We now have detailed knowledge of the hard X-ray spectrum and valuable information on the spatial structure of the hard X-ray sources. However, we do not have convincing measurements of the linear polarization of the bremsstrahlung. Polarimetry would yield direct information on the directivity (that is, anisotropy) of the emitting electron population and so provide constraints on the acceleration mechanism. Polarization measurements can also be used to distinguish between thermal and nonthermal sources, a task that is often not possible by other means, especially in the intermediate energy range (~10-50 keV) where the thermal and nonthermal contributions to the total X-ray flux can be similar.

Solar flare hard X-ray polarimetry is now at a nexus, where we are finally seeing the onset of observations capable of testing the numerous theoretical predictions that have existed in the literature for decades. The few existing polarization measurements are intriguingly different, yet collectively they suggest that the **magnitude** of the polarization vector is of the order predicted by models with strong anisotropy of the emitting electrons. However, the measured **orientation** of this vector may not be along the local solar radial, as predicted by most solar models. This raises the fascinating possibility that significant refinement of our models for particle acceleration and transport in solar flares may be required.

The cross-section for bremsstrahlung emission depends on the polarization state of the emitted photon either perpendicular to, or parallel to, the plane containing the pre-collision electron velocity vector and the photon emission direction [Gluckstern 53]. Taking into account that the accelerated electrons spiral around guiding magnetic field lines, one customarily transforms [Haug 72] the polarization state resulting from a given electron collision from the collision plane to a fixed plane defined by the guiding magnetic field and the photon emission direction, i.e. the line-of-sight to the observer. Convolution of the result with the energy spectrum and angular distribution of the emitting electrons results in an overall polarization signature either perpendicular to, or parallel to, the fixed plane. In general, the magnetic field that defines the axis of symmetry of the problem is taken to be the solar vertical, so that the fixed reference plane projects onto the radial direction on the solar disk. Predicted polarization vectors perpendicular to the reference plane (an azimuthal direction on the projected solar disk) are, by convention, denoted as positive, while polarization vectors parallel to the fixed reference plane (a radial direction on the projected solar disk) are denoted as negative.

Numerous authors have constructed a variety of solar flare models to calculate the expected polarization degree and orientation. They have incorporated different source geometries, electron energy spectra, and angular distributions. They have invoked both propagation of nonthermal electrons into a thick target [for example, Brown 72, Henoux 75, Langer 77, Bai 78, Leach 83, Leach 85], emission from a thermal source with a nonuniform temperature structure [Emslie 80], and a combination of the above [Emslie 80]. Models involving the downward beaming of accelerated electrons generally predict a predominantly negative (radial) direction for the polarization vector in the deka-keV photon energy range, with magnitudes of a few percent to a few tens of percent, depending on a variety of circumstances such as the atmospheric density and magnetic field model, but mostly on the assumed degree of downward anisotropy of the emitting electrons. Until recently, the only published model which predicted a non-radial polarization vector is an analysis of polarization from an extended thermal source, in which the required anisotropy of the electron distribution is driven by the temperature gradients in the source [Emslie 80]. In that model, the emission arises from the upper sections of an extended curved loop, so that the vertical direction (and the associated radial line on the solar disk) no longer has any special significance. Hence the polarization vector could be oriented at various angles to the radial direction (see Figure 3 of [Emslie 80]).

Measurement of solar flare hard X-ray polarization began in the 1970s with a series of measurements from the Russian Intercosmos satellites [Tindo 70, 72a, 72b, 73]. However, the reliability of these pioneering measurements has been questioned [Brown 74]. Attempts to measure solar hard X-ray polarization from a Space Shuttle payload were similarly inconclusive due to contamination of the lithium scatterer [Tramiel 84]. The next two decades saw little further progress in the area of solar flare hard X-ray polarization measurements, and there was a pervading doubt about the wisdom of dedicating a spacecraft instrument to polarization measurements, in part due to a growing suspicion that the inhomogeneity associated with a complex source geometry would render the actual polarization signature so small as to be undetectable.

Recognizing this critical lack of polarization data with which to test the growing plethora of theoretical predictions, limited non-imaging polarimetery was added to the RHESSI instrument [McConnell 02] as

a small beryllium scatterer added to the detector tray. Photons can scatter off this target into the rear segments of the four nearest-neighbor germanium detectors.

Using this capability, a hard X-ray polarization signal in the large (GOES class X4.8) flare of July 23, 2002 has been reported [McConnell 06]. This work reports a polarization of 15.4 ± 4.3%, oriented at an angle of 79 ± 4^{o} counterclockwise from the x-axis (defined as solar west). This flare was located near the East limb (at S13E72) and exhibited many of the characteristics normally associated with nonthermal electron acceleration and propagation, such as a hard power-law photon spectrum (γ~1.6) at high energies [Holman 03] and the appearance of bright hard X-ray footpoints with temporally-correlated spectra [Emslie 03].

The measured magnitude of the polarization is broadly consistent with the predictions of existing solar flare models that invoke the precipitation of a nonthermal electron beam into a dense chromospheric target, showing that, in this event at least, the polarization signal is not washed out due to source inhomogeneity, as had been feared. However, the orientation of the polarization vector is somewhat problematic, inasmuch as, given the ~195^{o} position angle of the event, the observed polarization is at an angle ~64^{o} to the local solar radial direction, considerably at variance with the ubiquitous prediction of a radial polarization vector. However, it should be remarked that surprisingly strong and consistent gamma-ray line redshifts in this near-limb event have been reported [Smith 03], indicating that the magnetic field guiding the trajectories of the emitting particles might be significantly non-vertical. Noting this possibility, Emslie *et al.* have explored the effect of loop tilt on the orientation of the predicted polarization vector [Emslie 06]. They found that not only did a much wider range of polarization vector orientations result for non-vertical guiding fields, but also that adding a loop tilt of the magnitude suggested by gamma-ray line observations [Smith 03] could indeed plausibly account for both the magnitude and the orientation of the observed polarization vector.

RHESSI's primary Ge detectors also act as active scatterers at higher photon energies (>200 keV), and correlation of the counts in adjacent detectors can be used to infer the incident polarization state. Hard X-ray polarization in two flares measured from such detector-detector correlations have been reported [Boggs 06]. In one event the polarization vector is approximately radial, in the other transverse.

Bogomolov reported extremely large polarizations (up to 70%) in a flare on October 29, 2003, using an experiment on the CORONAS-F satellite [Bogomolov 04]. This polarization value is far larger than predicted by any model hitherto proposed and indeed is at the limit of what can be expected from a model with 100% anisotropy in the emitting electron population. Although the validity of this result is brought into question by the fact that the same instrument recorded null results (upper limits of order 10%) for two other flares on October 28 and November 4, 2003, a confirmation of this very high polarization signal would be a very powerful constraint on flare models.

RHESSI's lack of an imaging polarimeter is a key deficiency since significant bremsstrahlung emission is accompanied by significant angular scattering of the emitting electrons [Leach 85]. Therefore, an otherwise measurably large polarization signature from one part of the source may be diluted by relatively unpolarized emission from another part. Measuring the polarization from different spatial locations in the flare hence provides a much more discriminating diagnostic on the anisotropy of the accelerated electrons. Consequently, imaging X-ray polarimetry will be a quantum leap in

capability that will resolve many of the current ambiguities and outstanding questions.

2.1.2 Instrument Requirements

The instrumental requirements are driven by our goal of imaging X-ray polarization measurements in solar flares with a balloon-borne instrument. The primary instrumental requirements are on imaging and polarization sensitivity.

Imaging at the 10 arc-second level is key to distinguishing the polarization signal from different parts of the flare, e.g., the foot points form the loop top. At solar maximum, there are on average four M-1 or brighter flares per day. An instrument must be able to measure polarization at the few-percent level in M-class flares to have a high probability of success in a single flight.

The polarimeter concept we propose meets these requirements by having sufficiently large area and high quantum efficiency to be a suitable detector for an imager using a rotating modulated collimator, and by having its peak sensitivity in the 20-50 keV band, where the nonthermal flare emission is brightest.

2.2 Technical Approach

We will meet our objective by building and testing a new type of photoelectric polarimeter that works by imaging the tracks of the photoelectrons to determine their emission angles on a photon-by-photon basis. This detector will be a prototype of a unit that would be one of four in a larger flight instrument. This work will leverage off our recent and ongoing work in soft X-ray polarimetry and micropattern detector technology [Black 03a, 03b].

2.2.1 Technical Rationale

We choose this type of polarimeter because it can have the largest effective area in the 20-50 keV band, the energy range of interest. The detector area is scalable because the same active medium is both the target and the detector.

In the following sections, we motivate the pursuit of photoelectric polarimetry. Then we describe photoelectric polarimeters based on gas micropattern proportional counters, and our recently demonstrated variant of this technique, the time-projection polarimeter (TPP), which presents the best option for scaling to large effective areas in the hard X-ray band. We then present recent results from the TPP. Finally, we estimate the sensitivity of a TPP as a balloon payload at the next solar maximum.

2.2.1.1 Photoelectric Polarimetry

In the X-ray energy range of interest for polarization measurements of solar flares (above ~20 keV), photons can interact by two physical processes, the photoelectric effect and Compton scattering. In both processes, the photoelectrons or Compton scattered photon of the initial X-ray interaction are emitted with a polarization-dependent angular distribution modulated as $cos^2\phi$, where ϕ is the azimuth angle measured from the electric vector in photoelectric interactions and from perpendicular to the electric vector in Compton interactions. The amplitude and phase of this modulation provides a measure of the amplitude and phase of the X-ray linear polarization. The instrumental challenge is to measure the azimuthal direction of the photoelectron or the Compton scattered photon.

Compton scattering becomes favored at energies above about 50 keV as the Compton cross-section begins to dominate the photoelectric in common detector materials. Solar X-ray polarimeters flown so far, RHESSI being the latest example, have been Compton instruments with a passive low-Z scatterer surrounded by multiple X-ray detectors. Above 50 keV, the technique can be improved by using active scatterers that detect the knock-on electron as in the Gamma Ray

Polarimeter Experiment (GRAPE) [McConnell 03].

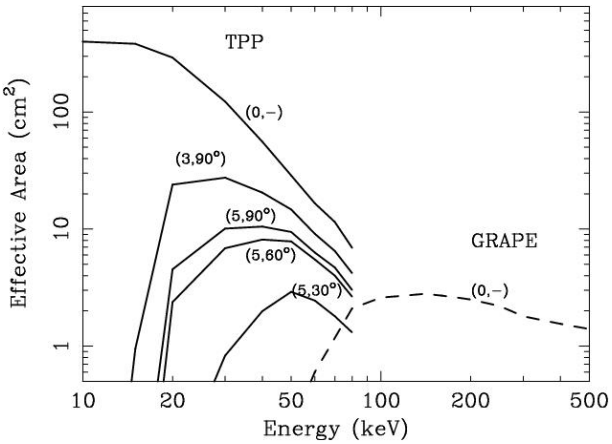

Figure 1: Photoelectric and active Compton polarimeters are complementary techniques. The effective areas of GRAPE and our photoelectric polarimeter concept, described in Section 2.2.1, are shown. The first number labeling each curve is the atmospheric overburden in g cm^{-2}. The second is the elevation of the Sun. The curves labeled (0,-) are on-orbit effective areas. None of the effective area calculations includes an RMC.

Below 50 keV, photoelectric polarimetry is an attractive technique that has become practical in the last few years. Interest in astronomical X-ray polarimetry in the soft X-ray band has been revived by the development of a highly sensitive measurement technique based on the photoelectric effect, using pixelized micropattern proportional gas detectors (MPGDs) [Costa01, Black03a, Bellazinni04]. These detectors have been demonstrated as highly sensitive polarimeters in the 2-10 keV band and can be optimized for higher energies, providing the possibility of hard X-ray imaging polarimetry.

The MPGD makes photoelectric polarimetry possible with pixels that are small (~100 microns) compared to the photoelectron path length (~1 mm). MPGDs can image the tracks of photoelectrons across many pixels along with a measurement of the energy lost in each pixel, a quantity directly related to the kinetic energy of the photoelectron. With this information, the photoelectron emission direction can be determined on an event-by-event basis.

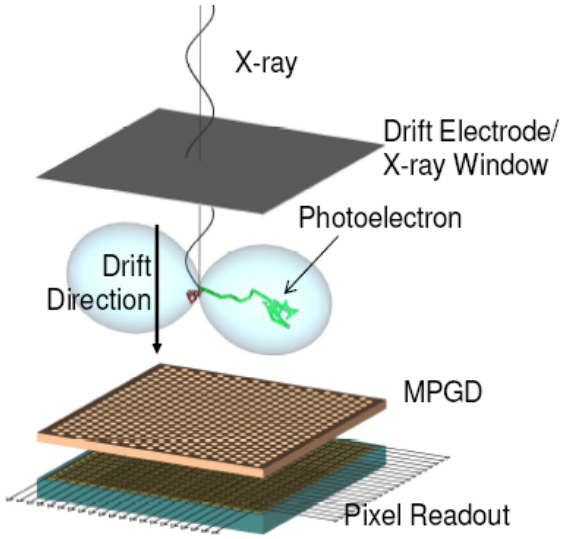

Figure 2: Pixelized micropattern polarimeter concept. The blue balloons represent the angular differential emission cross section.

As a result of photoelectric absorption, the atom ejects a photoelectron, preferentially in the direction of the photon's electric field with a $sin^2\theta\, cos^2\phi$ probability distribution, where θ is the polar angle and ϕ is the azimuth angle. In an MPGD, the photoelectron leaves a trail of ionization along its path that drifts to the pixelized detector under the influence of an applied electric field (Figure 2). In the MPGD, electron avalanches amplify the primary ionization, resulting in a record of the track that spans multiple pixels. Reconstruction software analyzes each track image and estimates the interaction point and the photoelectron emission angle. Thus, this photoelectric polarimeter is simultaneously sensitive to all phases of polarization and does not require rotation. Such a photoelectric polarimeter would provide a powerful tool for solar flare investigations by combining large effective area, low systematic errors, low background, and good energy resolution.

Photoelectric polarimeters offer large effective area for several reasons. First, the polarimeter can be made with a large physical

area that is homogeneous. That is the absorption medium and detection medium are the same, not divided between scatterer and detector. Second, the photoelectric effect is a perfect polarization analyzer in that every absorbed photon contributes to a 100% modulated distribution. With Compton scattering, the magnitude of the modulation is maximized only for scattering angles near 90 degrees. Third, the photoelectric polarimeter can have high quantum efficiency by using high-Z gases with significant depth and pressure.

The photoelectric polarimeter is also information-rich, which allows for sophisticated analysis of each event that optimizes sensitivity and reduces background and systematic errors. The electron track images are self-contained so that the emission angle can be reconstructed without *a priori* knowledge of the interaction point. Therefore, symmetry around the line of sight is not required to avoid false modulation. This also allows the analysis parameters to be optimized after the fact, and provides for the reliable rejection of background and charged particles events.

The energy resolution is significantly better than that of most solid-state detectors envisioned for the Compton scatter polarimeter. This may be a significant advantage if there are narrow lines in the background spectrum and provides the added bonus of high-resolution spectroscopy that is critical in measuring the often very steep (γ>7) solar flare spectra.

2.2.1.2 Time Projection Polarimeter (TPP)

The pixel MPGD photoelectric polarimeters demonstrated to date are small devices, about one cm^2, intended for the focal plane of an X-ray optic in the 2-10 keV band. In addition to polarization sensitivity, these detectors also have the important capability to form an image at the optic's focal plane. Even though the tracks extend over many pixels, potentially blurring the image, there is enough information in the tracks to be able to accurately identify the X-ray interaction point.

A hard X-ray polarimeter that uses a rotating bi-grid modulation collimator for imaging requires instead a large effective area and does not use focal plane imaging. The pixelized MPGDs we have demonstrated use technologies that could be scaled to the large areas required for an imaging solar flare polarimeter [Black03a, Black03c]. However, we have more recently demonstrated a new photoelectron track imaging technique using MPGDs that sacrifices focal plane imaging for a simpler readout that more readily scales to the large effective areas needed for hard X-rays.

This new technique works in fundamentally the same way as the pixelized detector, but forms the track image with a time-projection readout technique (Figure 3). This readout forms virtual pixels from a strip detector by deriving one pixel coordinate from the strip location and the orthogonal coordinate from the charge arrival time. While time-projection techniques are well established [Blum 93], they have not before been applied to photoelectric polarimetry.

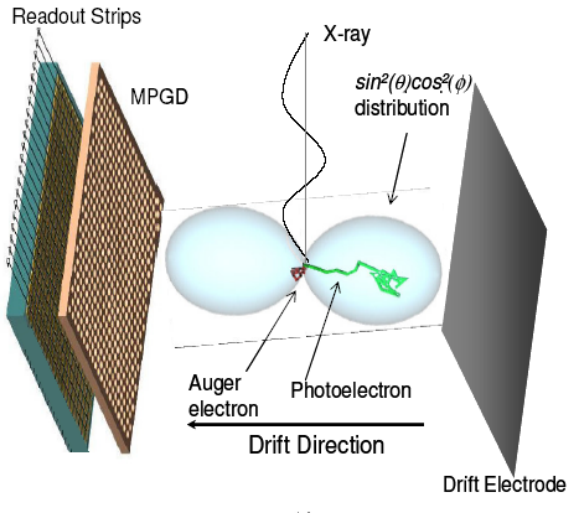

Figure 3: The time projection polarimeter uses a simple strip readout to form pixelized images of photoelectron tracks.

In the TPP, the MPGD detection plane is parallel to the incident X-rays and the readout is composed of strips that are individually instrumented with transient digitizers to measure both the amount of charge and its arrival time (Figure 3). Position information normal to the strips is determined by the arrival time of individual clusters of primary ionization. The hit strip number and arrival time then give the coordinates of a virtual pixel. Unlike a pixelized readout, the technologies involved in the micropattern TPP readily and inexpensively scale to large effective areas. The micropattern detectors, namely gas electron multipliers (GEMs) have been produced in very large areas for particle physics experiments. The readout electrodes can be produced with standard printed circuit technology and a very large detector can be read out with a small number of channels of commonly used nuclear electronics.

2.2.1.3 Demonstration TPP

As a demonstration of both the time-projection technique as an X-ray polarimeter and of the simplicity of the design, we recently built and tested a micropattern TPP in our laboratory using readily available off-the-shelf components. We used the device to measure both polarized and unpolarized 6 keV X-rays in a low-Z gas (40% neon, 60% dimethyl ether, DME). We also collected photoelectron tracks from 22 keV interactions in a gas more appropriate for hard X-ray polarimetry (70% Argon, 30% DME).

The TPP consists of a gas electron Figure 4multiplier (GEM) [Sauli 04] with 75 micron holes on a 150 micron, hexagonal pitch. About 0.5 mm beneath the GEM are 2.5 cm long readout strips on a 132 micron pitch that are aligned with the GEM holes along one of its 60^{o} symmetry axes. About 2 cm above the GEM is a drift electrode that bounds the third dimension of the active volume.

There are five sets of 24 strips giving a total active area of about 2.5 cm x 1.6 cm. Every nth strip in each set of 24 are connected together and to an analog-to-digital converter through a charge-sensitive amplifier. In this way, the entire active area with 120 strips can be read out with a single set of 24 electronics chains. As long as the valid electron tracks cross fewer than 24 strips, the tracks can be reconstructed without confusion. This scheme can be expanded indefinitely in both length and width (number of sets of strips). In our case, a typical track crosses about 8 strips.

Photons enter the detector in a direction parallel to the readout strips (the z direction). Photoelectrons and Auger electrons from X-ray interactions are emitted with a probability distribution peaked in the x-y plane

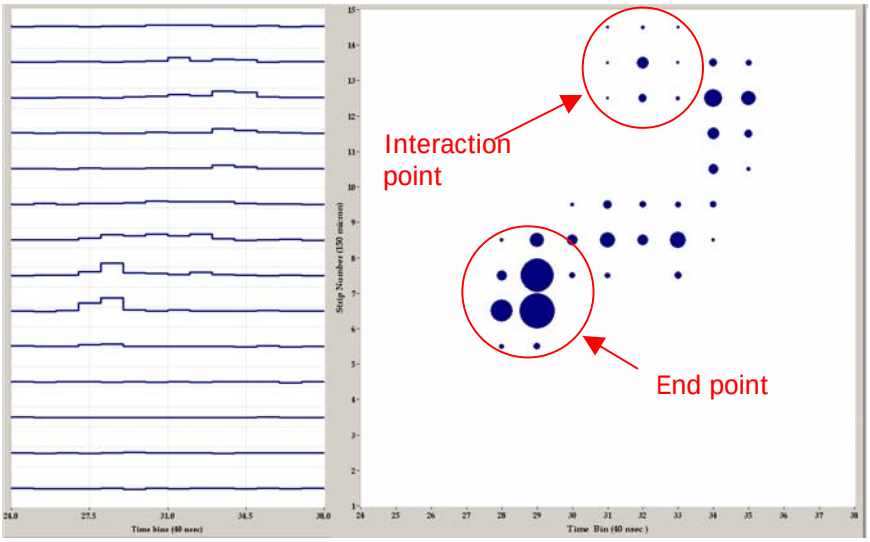

Figure 4: The TPP forms an image by digitizing the signal on each anode strip. Signal proportional to the charge deposited on each strip are shown on the left. The resulting image on right shows the interaction point, emission angle, and end of the track. Each circle has a size proportional to the deposited charge in each virtual pixel. The circles are on a 130 micron spacing.

and leave a trail of secondary ionization in their paths. The secondary ionization drifts along the y direction until it reaches the GEM, where the signals are amplified and collected on the readout strips. Images are formed by measuring the relative positions of deposited charge in x and y, x being the relative strip number location and y equal to the arrival time multiplied by the drift velocity. Note that only relative positions along the tracks are measured, which is all that is required to reconstruct the emission angle.

Figure 4 shows an example of a 6 keV photoelectron track imaged in this manner. The A/D converters act as waveform digitizers and are triggered by a signal from the GEM cathode. On the timescales of interest, the response of the charge-sensitive amplifiers is a step function, so that the charge in a time bin n is calculated simply as $Q_n = V_n - V_{n-1}$, where V_n is the digitized voltage at time bin n. Image pixels are defined by a strip number (x) and a time bin (y).

The non-uniform ionization density reveals details about the X-ray interaction. Most of the charge is deposited at the end of the photoelectron track. At the beginning of the track is a smaller cluster of charge deposited by the Auger electron, which is emitted isotropically.

The response of the TPP was first tested by exposing it to 6 keV X-rays polarized by scattering at 90° from a silicon crystal. Data were taken with the phase of polarization oriented approximately at 0°, 45°, and 90° with respect to the detector. The fill gas was DME at a pressure of 500 Torr.

The data were analyzed by reconstructing the emission angle of each photoelectron as the direction of the major axis of the second moment of the charge distribution about its barycenter [Black 03a]. Histograms of the emission angles were then fitted to the expected functional form:

$$N(\phi) = A + B\cos^2(\phi - \phi_0),$$

where ϕ_0 is the angle of the plane of polarization. The sensitivity to polarization is defined by the modulation:

$$\mu = (N_{max} - N_{min})/(N_{max} + N_{min}) = B/(2A + B),$$

where N_{max} and N_{min} are the maximum and minimum of the function, respectively.

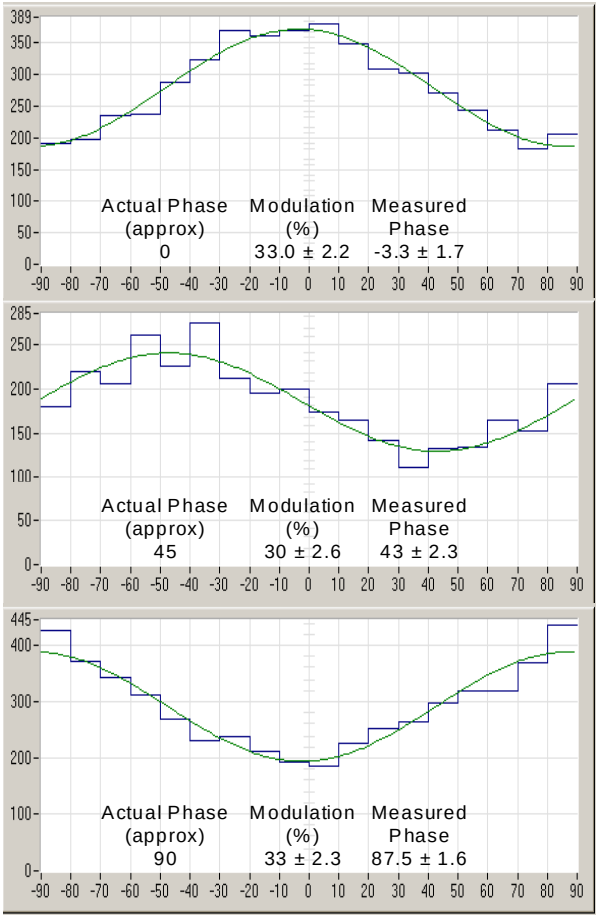

Figure 5: Histograms from polarized X-rays with phases of 0, 45, and 90 degrees. The lines are the list-squares fits to the data. Indicated uncertainties are one sigma.

The results, shown in Figure 5, demonstrate the uniform sensitivity of the TPP with respect to polization angle. The data fit the expected functional form and show consistent modulations with an average value of 32% at the expected angles.

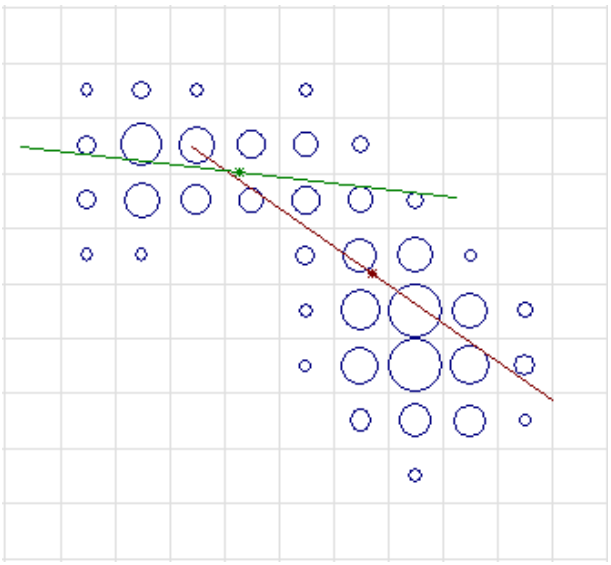

Figure 6: The two-stage angle reconstruction of a 6 keV X-ray. The red line shows the first-stage reconstructed track angle using the entire track. The green second-stage estimate is significantly more accurate.

A more sophisticated analysis technique enhances the polarization sensitivity by using only the information near the interaction point, where the angular information has been least affected by scattering [Pacciani 03]. This is a two-step analysis that first estimates the emission direction as before. The second step then repeats the calculation using only those pixels on the lower-density side of the original barycenter. Figure 6 shows an individual event with the first and the second, more accurate, iteration reconstructed angles.

Results using such an analysis on polarized and unpolarized 6 keV data are shown in Figure 7. The data were taken under identical conditions and analyzed with the same technique using the same analysis parameters. The unpolarized data are consistent with no modulation, but now the polarized data show a 51% modulation. These results are comparable to those obtained with pixel devices, but we note that the new device has more than a factor of 2 greater quantum efficiency than previously demonstrated pixel devices.

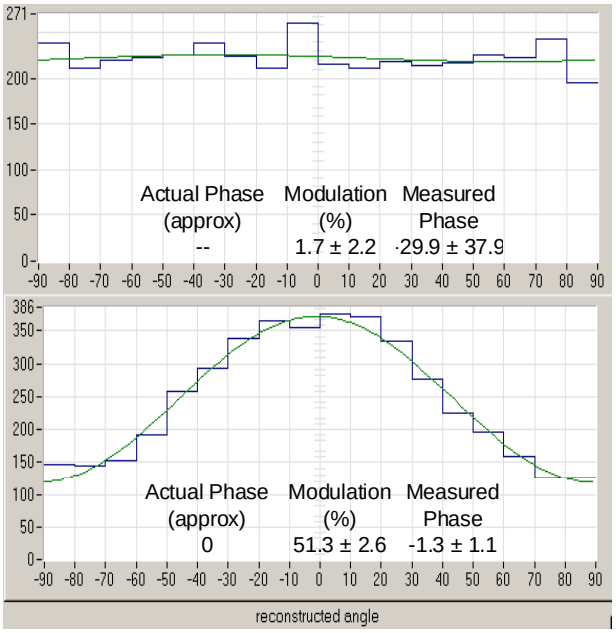

Figure 7: The two-stage reconstruction algorithm increases polarization sensitivity from 32% to 51%.

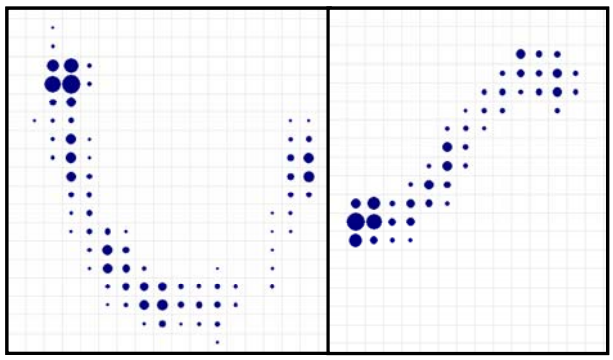

Figure 8: Examples of 22 keV tracks from Cd-209 in 600 Torr of Ar.

2.2.1.4 Sensitivity

In this section we outline the techniques we use for the calculation of polarization sensitivity. We will then apply these to a notional balloon instrument, and show that this design promises more than an order-of-magnitude increase in sensitivity to flare polarization over existing instruments.

Sensitivity Estimation Techniques

We have written detector simulation and track reconstruction code that predicts the sensitivities of various polarimeter configurations. The software reproduces

measured modulations at 4.5 and 6 keV, and produces results in agreement with similar simulations [Bellazzini 04]. The code simulates a photoelectron emitted with a $\sin^2\theta\cos^2\phi$ probability distribution and an isotropically distributed Auger electron. The two electrons propagate through the detector gas according to a single scattering model developed for electron microscopy [Joy 95]. To accurately model scattering below 10 keV, the simulation uses tabulated Mott cross-sections to calculate inelastic scattering and a modified Bethe-Block formula to calculate the energy loss. Ionization electrons produced along the track are propagated with diffusion through the drift region to the GEM. Each ionization electron produces an avalanche with proportional counter statistics. The avalanche electrons are each assigned to a virtual detector pixel.

The photoelectron track reconstruction algorithm follows a prescription given elsewhere [Pacciani 03]. The code identifies the interaction point with the end of the track with the least ionization density. It then estimates the photoelectron emission angle by calculating the major axis of the second moment of the charge distribution, considering only those pixels within a predetermined radius from the interaction point. As described in Section 2.2.1.3, the modulation factor is determined from a histogram of the emission angles for many photoelectrons. The modulation factor $\mu(E)$ is weighted by the number of events per unit energy, considering the source spectrum detector quantum efficiency, and collimator transmission. Finally, the broadband modulation factor $<\mu>$ and the expected number of source counts is used to calculate the MDP.

Because the measured modulation can never be negative, even an unpolarized source can give an apparent positive polarization. The sensitivity of a polarimeter is therefore expressed as the *minimum detectable polarization* (MDP), a polarization result that is statistically unlikely to arise from an unpolarized source. The MDP is a function of instrumental properties as well as the source strength, *S,* and the observing time, *t*. At the 99% confidence level,

$$MDP = \frac{4.29}{\varepsilon\mu SA}\left(\frac{\varepsilon SA + B}{t}\right)^{\frac{1}{2}}$$

where ε = quantum efficiency, A = collecting area, and B = background rate.

In the strong source approximation $S >> B$, the MDP scales with instrument parameters as $1/\mu\sqrt{\varepsilon A}$. We make the reasonable assumption for bright solar flares that this approximation is valid for an instrument with a suitable shield. The quantity $\mu\sqrt{\varepsilon A}$ may be used as an instrumental figure-of-merit dependent on detector dimensions, gas, pressure etc.

Instrument Concept

In this section we calculate the sensitivity of a notional balloon instrument, Figure 9, consisting of four polarimeters each behind a RMC, and discuss factors in its optimization. The basic factors affecting the sensitivity of a TPP are the fill gas and its pressure, the GEM area, the distance between drift electrode and GEM, and the readout pitch. Schematically, we choose the detector parameters by first selecting a fill gas, then modeling modulation as a function of X-ray energy, anode pitch, and drift distance. We then consider the GEM area, which determines in instrument's effective area. Finally we consider a realistic flare spectrum and calculate sensitivity as a function of solar altitude for possible balloon float altitudes and latitudes.

Choosing a fill gas requires considering drift speed, diffusion, and mean atomic number. A gas with low drift velocity is desirable to achieve high photoelectron spatial resolution with relatively low-speed low-

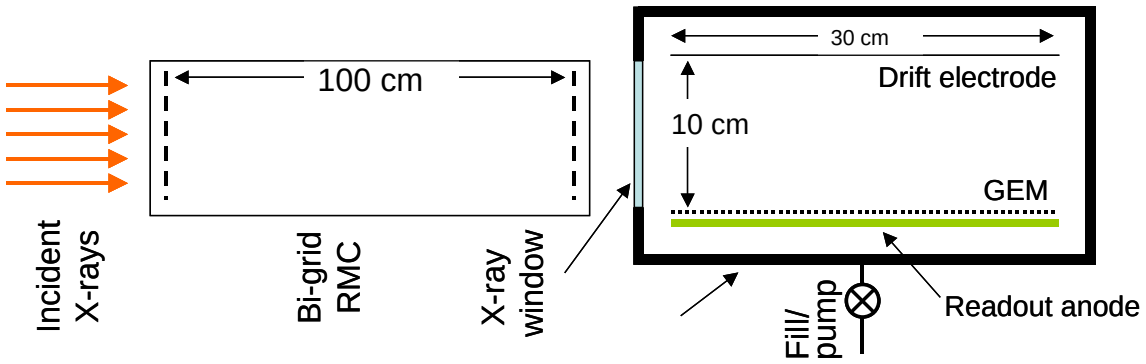

Figure 9: The imaging polarimeter concept has four detector units, each using a bi-grid RMC for imaging and a TPP with 10 x 10 cm^2 aperture.

power electronics. A gas with low electron diffusion allows a large drift distance, reducing the area of GEM and fine-pitch anode required to achieve a particular effective area. Increasing atomic number increases stopping power and therefore the quantum efficiency of a detector for a given size and gas pressure. But increasing Z also increases the number of inelastic scatters compared to elastic scatters, making it harder to reconstruct the initial direction of the photoelectron. Further, the incident X-ray energy must be at least twice the K-shell energy of the absorber in order to produce a large modulation. This constraint and increased scattering eliminates xenon-based gases for a 20-80 keV polarimeter, but argon and krypton meet the criteria.

A 70%/30% mixture of argon and dimethyl ether (DME) appears to be the best fill gas. A mixture of Kr and DME might be superior if better algorithms are devised to reconstruct the highly scattered tracks, and complications from krypton's high fluorescence yield can be addressed. Also, a negative ion drift proportional counter using CS_2 as the charge-carrying ion is attractive for its extremely low diffusion and drift speed. We recently received Goddard internal funding to investigate the reduction in diffusion using this gas. However, it is not clear if negative ion counters can be fast enough to track the rapid temporal modulation produced by the RMCs.

For a 70%/30% Ar/DME gas combination, we modeled detectors with different gas pressures, drift distances, and readout pitches and selected the parameters which maximize sensitivity, Figure 10. Based on this study, we selected a pressure of 3 bar, a drift distance of 10 cm and a 200 μm pitch readout for the flight detector concept. A 200 mm pitch readout was selected since this is within the capabilities of many printed circuit board manufacturers and there is little benefit to finer pitch.

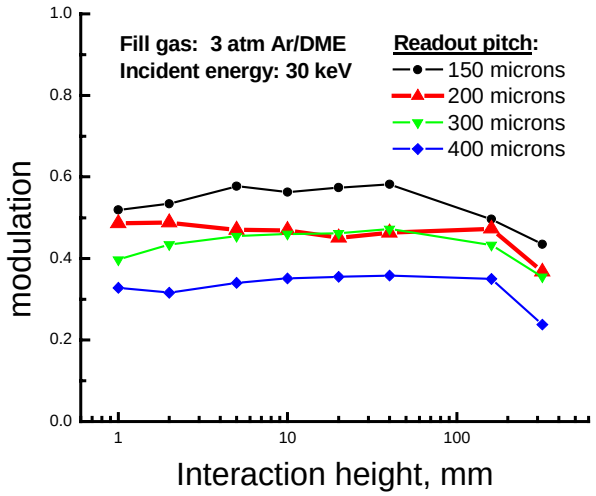

Figure 10: Simulated modulation at 30 keV. The modulation is approximately independent of drift distance for distances less than 10 cm.

The depth of the baseline design is 30 cm, yielding a quantum efficiency of 25% at 30 keV. Deeper units should be feasible, but in

our judgment, a 30-cm unit can be built without significant risk or large expenditure.

Baseline detector parameters	
Fill gas	70% Ar, 30% DME
Fill pressure	3 bar
GEM & anode area	10 cm x 30 cm
GEM pitch	150 microns
anode pitch	200 microns
GEM-anode separation	0.1 cm
Drift-GEM separation	10 cm
Readout channels	24

Table 1: Detector parameters of the balloon instrument. These parameters are the same for the prototype detector to be built for the proposed work.

The detector *dead-time* in reading an event is the elapsed time for the entire photoelectron track to drift into the GEM and onto the readout anode. The 70%/30% Ar/DME mixture has a drift velocity of ~5 cm/μs, so for a typical 50 keV track length of 3 mm, the dead time on the order of 1.5 μs. This is well within the requirement, since an X-class flare will produce less than 1000 events per second in each detector. The *delay* between an X-ray interaction and its detection is determined by the drift distance. The drift height of 10 cm results in a maximum delay of 50 μs, far smaller than the ~2 ms requirement imposed by an RMC with 10 arcsecond locational ability rotating every 5 seconds.

The notional instrument has high polarization sensitivity in the 20-60 keV range (Figure 11). Figure 12 shows the instrument sensitivity integrated over 20-80 keV. The result of this calculation indicates that the instrument has the required sensitivity to measure X-ray polarization from even C-class flares in a single mid-latitude flight.

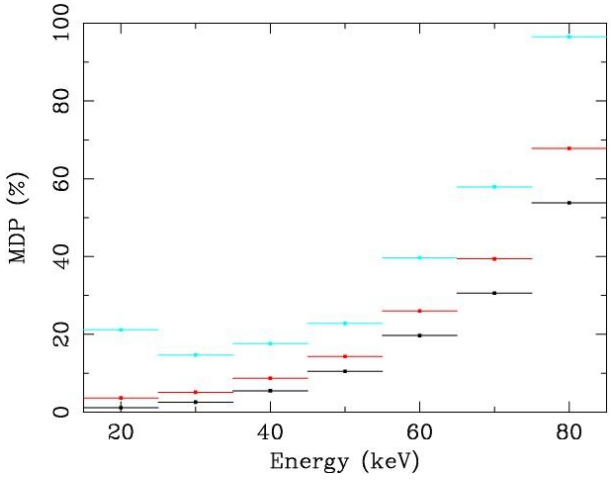

Figure 11: MDP per unit energy for an X-1 flare with an overburden of 5 g cm-2 at elevations of 90 (black), 60 (red) and 30 (blue) degrees. We assume an RMC with 25% transmission, an observation lasting 100 s, and an $E^{-4.3}$ spectrum. The MDP scales inversely with the square-root of the number of counts.

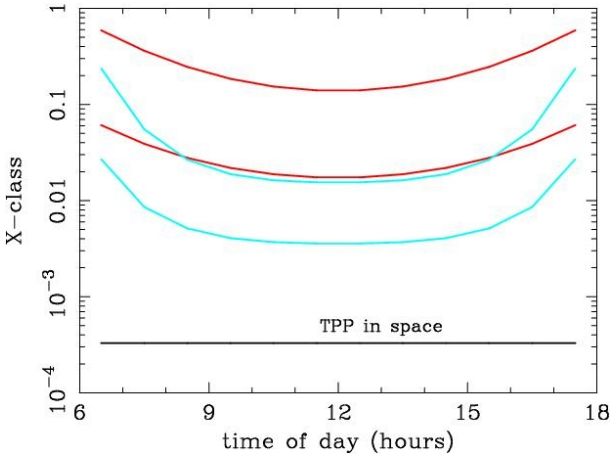

Figure 12: 10% MDP contours from 20 to 80 keV for launches from McMurdo (red) and Palestine (blue). In each case, the upper (lower) curves represent atmospheric overburdens of 5 (3) g cm^{-2}. The assumptions are the same as those for Figure 11.

2.2.2 Development Detector Unit

We propose to build a prototype detector unit based on the design described in the previous section and shown in Figure 9. The detector is operated as a sealed proportional counter inside a pressure

chamber. This simplifies the operation and some aspects of construction. However, sealed operation requires the use of low out-gassing materials and techniques similar to vacuum practices for the 10^{-6} Torr range in order for the gas diffusion and drift velocity to remain stable over days or weeks. Prior to operation, the chamber is evacuated with a turbomolecular pump.

The chamber also requires vacuum and pressure transducers, high-voltage feedthroughs for biasing the drift electrode and GEM, and low-voltage feedthroughs for signals and preamplifier power. We will fabricate an X-ray window for the chamber through which photons enter the active region between the drift electrode and the GEM. Inside the chamber, field-shaping electrodes surround the active region to eliminate false modulation arising from drift-field non-uniformity, creating an electric field that is uniform in magnitude to ~1% and in direction to a few degrees. To minimize out-gassing material, only the charge preamplifiers are mounted in the chamber.

At Goddard, we fabricate GEMs with 150-μm pitch by tensioning perforated metal foils in frames, and suspending them ~100 μm apart. Our demonstration polarimeter uses a GEM with this construction. These GEMs are very resilient with respect to electrical breakdown, and have superior outgassing properties because they have no plastic substrate. We plan to demonstrate the manufacture of GEMs large enough for the proposed prototype during the current fiscal year. GEMs with 140-μm pitch and 10 cm x 10 cm area are available from CERN. Three of these could be tiled in our detector. The CERN GEMs have copper electrodes adhered to a polyimide substrate that could be used if fabrication of tensioned GEMs on the scale of the detector becomes problematic.

We have chosen a pitch of 200 μm for the readout anode so it can be fabricated as a fine-line printed circuit board on a rigid substrate. The smaller demonstration polarimeter's readout anode is a fine-line printed circuit board with 130 μm pitch, showing the feasibility of this approach.

The flight concept TPC consists of 500 readout anode strips on a 200 μm pitch. The strips will be multiplexed into 25 readout channels by tying every 25th strip together, forming 20 groups of 25. No valid photoelectron tracks will span as many as 25 strips, so that events can be reconstructed without confusion.

We will use the same readout system used for our demonstration. The front-end readout consists of a charge-sensitive preamp followed by differential output amplifier for each readout channel. The preamps are based on current-feedback operational amplifiers that provide fast, low-noise, low-power charge sensitive amplifiers. A low-noise, wideband differential output amplifier (baseline Analog Devices AD8130) drives the signals to the A/D board.

The A/D board has a wideband differential receivers/amplifiers followed by an 8-channel, low-power (125 mW/channel, 50 MHz sampling) ADC as is used in our prototype. At the drift field strength that creates the minimum electron diffusion in Ar/DME, the electron drift velocity is ~6 mm/μs. So, 200 μm pixels will require 30 MHz sampling at that drift velocity. FPGAs drive the readout, store the data locally, and control communications. The readout is triggered by a zero-crossing discriminator using an amplified signal from the GEM cathode.

2.2.3 Testing and Calibration

Our goal is to demonstrate that the TPP systematics allow an MDP ~3% or less. We estimate modulations of approximately 0.5, so our goal translates to understanding the response to unmodulated X-rays to 1.5% at the 99% level of confidence.

We will perform initial testing in an established configuration used for optimizing 2-10 keV polarimeters. We will test the polarimeter with a Ne/DME mixture at a pressure of ~1 bar and with an existing 100% modulated 4.5 and 6 keV X-ray source.

We will measure the modulation as a function of energy, drift distance and pressure in the expected operating range by constructing a rotating 20-50 keV polarized source from scattering bremsstrahlung from an Oxford XTF-5011 50 keV X-ray tube off a beryllium or lithium hydride scatterer through ~90 degrees. We estimate a polarized flux of ~10 Hz with this arrangement; sufficient to make few percent measurements in the 20-30 keV band in tens of minutes.

Measuring the response to X-rays from radioisotope decay is the best end-to-end calibration in the laboratory, although it may be problematic for a fully configured flight instrument. We will measure the un-modulated response with unpolarized 60 keV X-rays from a one mCi ^{241}Am source, which is bright enough to allow a search for calibration variations on time-scales from minutes to days. We will also investigate other techniques that may be more suitable for in-flight calibration. One possibility is to use a cylindrically symmetric transmission anode X-ray source such as the Moxtex 40 keV Bullet. We will also compare the ^{241}Am results to techniques that directly measure the drift velocity, either with cosmic-rays or with electrons liberated from a Mg cathode in the active volume by a UV LED pulser.

2.3 Work Plan

The project will be directed by Principal Investigator, Brian Dennis. The PI and co-investigators responsible for the instrument are co-located at Goddard, facilitating rapid communication and decision-making. The PI will manage the program and act as the liaison between the instrument development work and the science objectives. Co-I Gordon Emslie will provide the scientific justification for imaging X-ray polarimetry of solar flares and monitor the instrument capabilities as they are developed to ensure that the scientific objectives can be met. Co-Is Philip Deines-Jones and Kevin Black will be responsible for all instrument design, development, fabrication, and testing activities. Collaborator Gordon Hurford will advise the polarimeter development team on the characteristics that will be required to implement an imaging capability using rotating bigrid collimators. Collaborator Robert Lin and his graduate student Amir Caspi will advise the team on instrument design considerations to ensure compatibility with future balloon and possible space flight opportunities.

Key activities and milestones are shown in the following schedule.

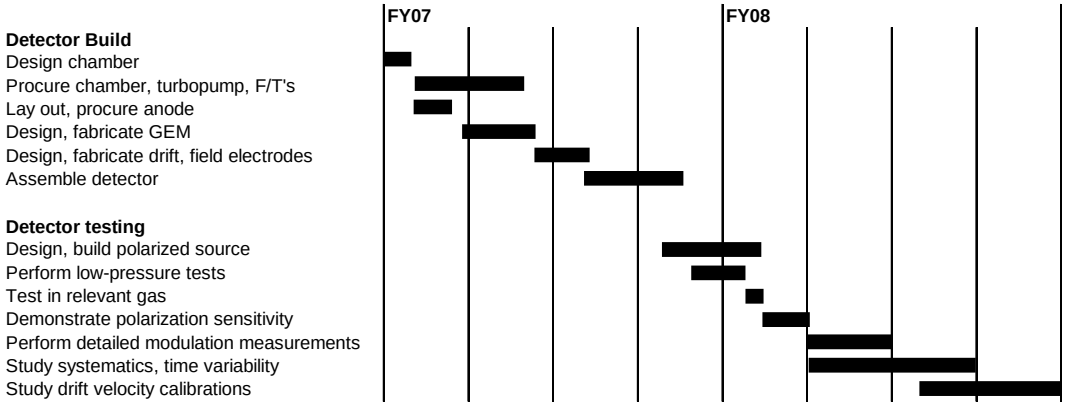

3 References

[Bai 78] Bai, T., & Ramaty, R. 1978, “Backscatter, anisotropy, and polarization of solar hard X-rays”, *Ap. J*., **219**, 705.

[Bellazzini 02] Bellazzini, R. et al., 2002, “X-Ray Polarimetry with a Micro Pattern Gas Detector with Pixel Read Out”, *IEEE Trans Nucl. Sci*., **49**, 1216.

[Bellazzini 04] Bellazzini, R. et al., 2004, “Reading a GEM with a VLSI pixel ASIC used as a direct charge collecting anode”, *Nucl. Instr. Meth. A*., **535**, 477.

[Black 03a] Black, J.K. et al., 2003, "X-ray polarimetry with an active-matrix pixel proportional counter", *Nucl. Instr. Meth., A*. **513**, 639.

[Black 03b] Black, J.K. et al., 2003, "The imaging X-ray detector for Lobster-ISS", *Nucl. Instr. Meth., A*. **513**, 123.

[Black 03c] Black, J.K. et al., 2003, " High Sensitivity X-ray Polarimetry with Amorphous Silicon Active-Matrix Pixel Proportional Counters”, *Proc SPIE,* **5165**, 346.

[Blum 93] Blum, W. and Rolandi, L. 1993, “Particle Detection with Drift Chambers,” Springer-Verlag, ISBN3-540-58322-X

[Boggs 06] Boggs, S. E, Coburn, W., & Kalemci, E. 2006, *Ap. J*., in press.

[Bogomolov 04] Bogomolov, A. V. et al. 2004, in *Multi-Wavelength Investigations of Solar Activity*, IAU Symposium No. 223 (eds. A. V. Stepanov, E. E. Benevolenskaya & A. G. Kosovichev), Cambridge: Cambridge University Press, p. 447.

[Brown 72] Brown, J. C. 1972, “The Directivity and Polarisation of Thick Target X-Ray Bremsstrahlung from Solar Flares”, *Solar Phys*., **26**, 441.

[Brown 74] Brown, J. C., McClymont, A. N., & McLean, I. S. 1974, *Nature*, **247**, 441.

[Costa 02] Costa, E. et al., 2001, "An efficient photoelectric X-ray polarimeter for the study of black holes ", *Nature*, **411**, 662.

[Emslie 80] Emslie, A. G., & Brown, J. C. 1980, “The polarization and directivity of solar-flare hard X-ray bremsstrahlung from a thermal source”, *Ap. J*., **237**, 1015.

[Emslie 02] Emslie, A. G., Kontar, E. P., Krucker, S., & Lin, R. P. 2003, “RHESSI Hard X-Ray Imaging Spectroscopy of the Large Gamma-Ray Flare of 2002 July 23”, *Ap. J*., **595**, L107.

[Emslie 80] Emslie, A. G., & Vlahos, L. 1980, “Radiation signatures from a locally energized flaring loop”, *Ap. J*., **242**, 359.

[Gluckstern 53] Gluckstern, R. L., & Hull, M. H., Jr. 1953, “Polarization Dependence of the Integrated Bremsstrahlung Cross Section”, *Phys. Rev*., **90**, 1030.

[Haug 72] Haug, E. 1972, ” Polarization of Hard X-Rays from Solar Flares”, *Solar Phys*., **25**, 425.

[H´enoux 75] H´enoux, J.-C. 1975, “Anisotropy and polarization of solar X-ray bursts “, Solar Phys., **42**, 219.

[Holman 02] Holman, G. D., Sui, L., Schwartz, R. A., & Emslie, A. G. 2003, "Electron Bremsstrahlung Hard X-Ray Spectra, Electron Distributions, and Energetics in the 2002 July 23 Solar Flare", *Ap. J.*, **595**, L97.

[Joy 95] Joy, D. C. 1995, "Monte Carlo Modeling for Electron Microscopy and Microanalysis" (Oxford Series in Optical and Imaging Sciences).

[Langer 77] Langer, S. H., & Petrosian, V., 1977, "Impulsive solar X-ray bursts. III - Polarization, directivity, and spectrum of the reflected and total bremsstrahlung radiation from a beam of electrons directed toward the photosphere", *Ap. J.*, **215**, 666.

[Leach 85] Leach, J., Emslie, A. G., & Petrosian, V., 1985, "The interpretation of hard X-ray polarization measurements in solar flares", *Solar Phys.*, **96**, 331.

[Leach 83] Leach, J., & Petrosian, V. 1983, "The impulsive phase of solar flares. II - Characteristics of the hard X-rays", *Ap. J.*, **269**, 715.

[Lin 02] Lin, R. P., et al. 2002, "The Reuven Ramaty High-Energy Solar Spectroscopic Imager (RHESSI)", *Solar Phys.*, **210**, 3.

[Martoff 00] Martoff, C. J. et al., 2000, "Suppressing drift chamber diffusion without magnetic field", *Nucl. Instr. Meth, A.*, **440**, 355.

[McConnell 02] McConnell, M. L., Ryan, J. M., Smith, D. M., Lin, R. P., & Emslie, A. G. 2002, "RHESSI as a Hard X-Ray Polarimeter", *Solar Phys.*, **210**, 125.

[McConnell 06] McConnell, M. L., Ryan, J. M., Smith, D. M., Hurford, G. J., Fivian, M., Lin, R. P., & Emslie, A. G. 2006, *Solar Phys.*, submitted.

[Pacciani 03] Pacciani, L. et al., 2003, "Sensitivity of a photoelectric x-ray polarimeter for astronomy: the impact of the gas mixture and pressure", *Proc SPIE,* **4843**, 394.

[Sauli 04] Sauli, F. 2004, "Progress with the gas electron multiplier," NIMA **522**, 93

[Smith 03] Smith, D. M., Share, G. H., Murphy, R. J., Schwartz, R. A., Shih, A. Y., & Lin, R. P. 2003, "Physical Implications of RHESSI Neutron-Capture Line Measurements", *Ap. J.*, **595**, L81.

[Tindo 72a] Tindo, I. P., Ivanov, V. D., Mandel´stam, S. L., & Shuryghin, A. I. 1972a, "New Measurements of the Polarization of X-Ray Solar Flares", *Solar Phys.*, **24**, 429.

[Tindo 72b] Tindo, I. P., Ivanov, V. D., Valni´cek, B., & Livshits, M. A. 1972b, "Preliminary Interpretation of the Polarization Measurements Performed on 'Intercosmos-4' during Three X-Ray Solar Flares", *Solar Phys.*, **27**, 426.

[Tindo 73] Tindo, I. P., Mandel´stam, S. L., & Shuryghin, A. I. 1973, "Further Polarization Measurements of the Solar Flare X-Ray Emission", *Solar Phys.*, **32**, 469.

4 Facilities and Equipment

This investigation makes substantial use of existing GSFC hardware and laboratory facilities. The GSFC Laboratory for X-ray Astrophysics has a fully equipped laboratory for the development and testing of micropattern gas detectors and photoelectric polarimeters. We have several pieces of equipment specifically designed for micropattern detector or polarimeter work:

- Gas filling and exhaust manifolds approved for handling flammable gases and equipped with a Nanochem filter for purifying DME,
- A 32-channel TPC readout system suitable for the proposed project,
- Detector simulation and event reconstruction software designed for photoelectric polarimetry,
- A NanoLED sub-nanosecond pulsed diode excitation system with 280 nm LED, suitable for liberating electrons from a photocathode for drift speed measurement, and
- Sources of 100% polarized 4.5 and 6 keV X-rays.

Our laboratory has several Oxford XTF-5011 50 keV X-ray tubes which can be used with a scattering target to make a source of 100% polarized high-energy X-rays. We have a NanoLED sub-nanosecond pulsed diode excitation system with 280 nm LED, suitable for liberating electrons from a photocathode to perform drift speed measurements. We also have radioisotopic X-ray sources, low-ripple HV power supplies and general laboratory equipment to carry out this work.

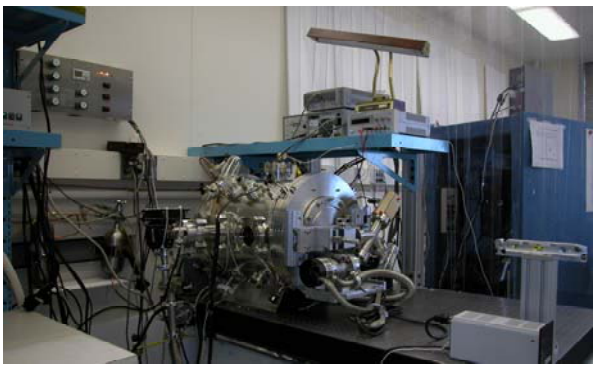

The 1-atm polarimeter test chamber has supporting readout electronics and a gas handling manifold approved for flammable gases that will be adapted for the proposed work.